NANO LETTERS

pubs.acs.org/NanoLett

Letter

Flexible Nanoporous Materials by Matrix Removal from Cylinder-Forming Diblock Copolymers

Hongyun Xu, Han Xiao, Christopher J. Ellison,* and Mahesh K. Mahanthappa*

Cite This: *Nano Lett.* 2021, 21, 7587−7594

Read Online

ACCESS | Metrics & More | Article Recommendations | Supporting Information

ABSTRACT: We describe a straightforward self-assembly route to nanoporous materials derived from a hexagonally-packed cylinder (HEX) morphology of a polyisoprene-*block*-polylactide (PI-*b*-PLA) diblock copolymer, by thermal cross-linking of the minority PI domains followed by selective chemical etching of the PLA matrix. The resulting mechanically stable and porous samples defy the expectation that the remaining cylinders cannot yield a robust, integrated material upon matrix removal. Scanning electron microscopy imaging reveals that this unexpected structural integrity stems from the interconnected nanofibrils therein, reflecting topological defects at the grain boundaries of the parent polydomain HEX nanostructure. Hydrodynamic radius-dependent poly(ethylene oxide) (M_n = 0.4−35 kg/mol) permeation behavior through these monoliths directly demonstrated the continuity and size selectivity of the nanoporous material. The ready accessibility of block copolymer HEX morphologies of varied chemistries suggests that this matrix etching strategy will enable the future design of functional, size-selective nanofiltration membrane materials.

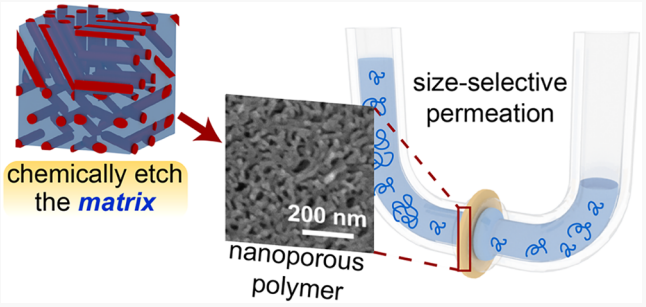

KEYWORDS: *nanoporous polymer, polymer membrane, nanofiltration, block copolymer, self-assembly*

The development of robust and scalable methods for fabricating nanoporous polymeric materials affects their applications in microelectronic device manufacturing,[1−4] size-selective separations membranes,[5,6] solid catalysts,[7−10] templates for porous inorganic materials,[11−14] and drug delivery vehicles.[15] While the fabrication of an isoporous polymer structure is crucial for many of these applications, periodic long-range translational order in the pore structure is often not an absolute requirement. Numerous applications instead require continuous and macroscopically percolating pores through the materials. In comparison to porous metals and ceramics, the pore sizes, pore wall functionalities,[16,17] interfacial wettability,[18] and overall mechanical properties of nanoporous polymers may be tailored by a judicious selection of their constituent monomers, their compositions, and their processing histories.[19] The melt and solution processabilities of monomeric or polymeric precursors into porous media further enhance the utility of the resulting materials, by enabling their fabrication in formats ranging from monoliths to thin film coatings.

An enticing, "bottom up" design strategy for producing nanoporous materials with pores of tailored dimensions decorated with well-defined chemical functionalities and tunable physical properties relies on block copolymer self-assembly.[16,20] Block copolymers, which are derived from covalently linking chemically dissimilar polymer segments, thermodynamically microphase separate into spherical, hexagonally-packed cylinder (HEX), gyroid, and lamellar nanostructures with microdomain dimensions that depend on the polymer composition and molecular weight.[21,22] Integrating mechanically robust (e.g., high T_g or cross-linkable) blocks and degradable segments into these nanostructured polymers allows the development of porosity by selective chemical etching of the nanodomains.[23−25] Register, Chaikin, and co-workers first demonstrated the formation of polymer-based nanolithography templates by ozonolysis of the polydiene domains of a self-assembled polystyrene-*block*-1,4-polybutadiene thin film.[1] By a conceptually related strategy, Hillmyer and co-workers produced isoporous PS monoliths with 15 nm diameter cylindrical pores, by flow-induced alignment of a HEX-forming polystyrene-*block*-polylactide (PS-*b*-PLA) diblock followed by saponification of the minority-phase PLA cylinders.[26] This approach has been extended using degradable polyether[27] and polysiloxane[28,29] segments. These methods produce materials with ordered nanopore arrays, albeit at the expense of nontrivial processing steps to produce pseudomonodomain morphologies.[2,20]

Received: May 28, 2021
Revised: August 11, 2021
Published: August 30, 2021

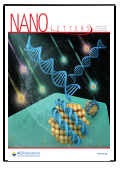

https://doi.org/10.1021/acs.nanolett.1c02097
Nano Lett. 2021, 21, 7587−7594

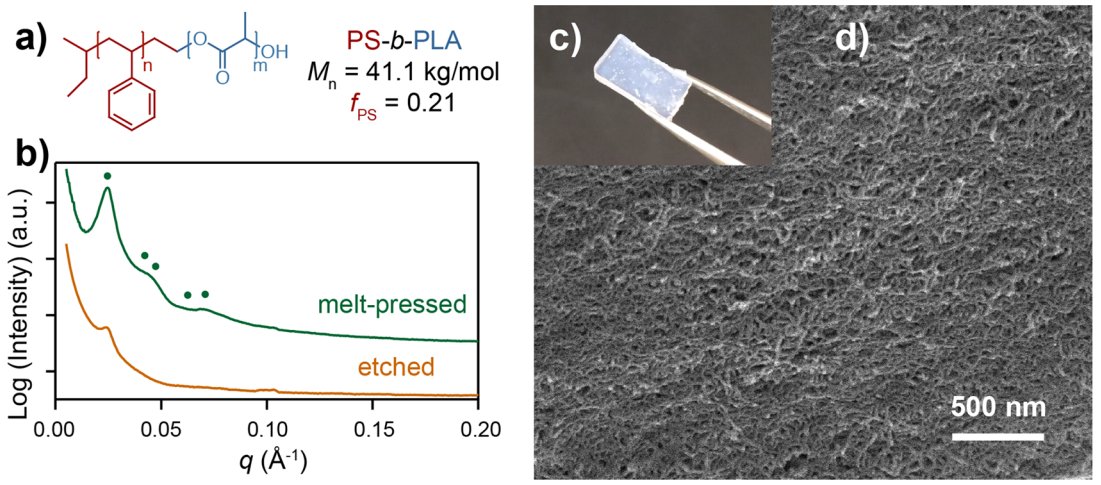

Figure 1. (a) Molecular structure of a PS-*b*-PLA block copolymer synthesized via tandem anionic and ring-opening transesterification polymerizations. (b) SAXS patterns of a compression-molded PS-*b*-PLA sample (green) and a water-infused monolith after PLA matrix etching (orange). Markers indicate the positions of the expected peaks for hexagonally packed cylinders with $(q/q^*)^2 = 1, 3, 4, 7, 9, \ldots$ with $q^* = 0.0244$ Å^{-1}. The etched PS-*b*-PLA sample (orange) exhibits only a single correlation peak at nearly the same q^* position as that before etching, indicative of short-range correlations (the peak at 0.10 Å^{-1} is an artifact arising from the sample holder). (c) Picture of the water-filled porous PS sample after etching and (d) SEM image of the cryofractured and vacuum-dried sample showing interconnected PS cylinders.

Selective chemical etching of bicontinuous block copolymer morphologies enables access to useful high surface area nanoporous materials, while avoiding arduous processing steps. Ordered and disordered bicontinuous nanoporous polymers have been derived from microphase separated double-gyroid morphologies[28,30,31] and bicontinuous microemulsions,[32] respectively. However, these privileged phases only form over narrow composition and molecular weight ranges that limit synthetic access and ultimate porosity.[31] Broader access to polymers with percolating, disorganized pores has been recently reported by polymerization-induced microphase separation (PIMS),[33−36] by cross-linking disordered states of diblock polymers above their order-to-disorder transition temperatures,[37−39] and through the formation of randomly end-linked copolymer networks (RECNs).[40]

A further limitation of many of the above routes to nanoporous polymers is that the observed porosity is typically ≤50%, as a consequence of the block copolymer composition presumed to furnish minimal mechanical integrity. While the selective degradation of HEX morphologies of linear AB diblock copolymers comprising structurally robust cylinders in a degradable matrix would be theoretically expected to yield higher-porosity nanostructures with matrix volume fractions as high as 65−75 vol %,[41] conventional wisdom suggests that matrix domain etching in such phases leads to weak materials that readily disintegrate. Such methods have indeed been reported as a route to narrow-dispersity nanotubes,[42,43] polymer nanofibrils,[44,45] and metallized nanowires.[46] In contrast to this conventional wisdom, we herein demonstrate that selective matrix domain removal from unaligned HEX morphologies of block copolymers yields mechanically robust, high-porosity polymers with defined pore sizes.

By a previously reported sequential anionic polymerization and Sn-catalyzed ring-opening transesterification polymerization (ROTEP) sequence,[26] we synthesized a PS-*b*-PLA diblock (Figure 1a) with total molecular weight M_n = 41.1 kg/mol ($Đ = M_w/M_n$ = 1.24) and a minority PS volume fraction, f_{PS} = 0.21 (see Figures S1a,b and S2a,b, for synthesis and characterization details). Synchrotron SAXS analysis of a 0.7 mm thick sample compression-molded at 120 °C exhibits a modestly ordered HEX morphology (Figure 1b), presumably due to the strongly segregated nature of this high molar mass polymer. Immersion of this material into 2.5 M NaOH in MeOH/H_2O (20/80 v/v) at 45 °C for 12 h completely degrades the PLA therein, evidenced by the absence of any PLA ^{1}H NMR resonances (δ 5.1−5.3 ppm in Figure S2b,c) upon dissolution of the etched sample in $CDCl_3$. The mass loss from the etched and vacuum-dried PS monolith was 80.9 wt %, in comparison to the 81.3 wt % theoretically anticipated from the copolymer composition. The resulting water-filled PS monolith surprisingly retains its original shape with a clear, slightly bluish appearance (Figure 1c), and it may be readily handled. This water-imbibed monolith was cryofractured in N_2(l), vacuum-dried, coated with a 2 nm thick Ir layer, and imaged by SEM to reveal the porous network of discrete, randomly oriented fibrils shown in Figure 1d. While a SAXS analysis of the etched samples (Figure 1b) corroborates the observed loss of long-range translational order, short-range correlations consistent with the ordered microdomain periodicity remain in the water-infused monolith. While the vitreous nature of the PS domains preserves the porous nanostructure after PLA removal, the low molecular weight of the PS segment (M_n = 7.7 kg/mol) confers little mechanical strength. Nonetheless, this finding establishes that the cylinders in this unaligned, polydomain HEX morphology are sufficiently interconnected to furnish an integrated nanoporous polymer monolith by matrix domain etching. This result is conceptually related to prior work by Bendejacq et al. that reported water-induced swelling without the disintegration of HEX-forming poly(styrene)-*block*-pol(acrylic acid) (PS-*b*-PAA) monoliths with a hydrophilic PAA matrix phase.[47] Furthermore, the disorganized cylinder morphology observed in Figure 1d is also reminiscent of that indirectly observed by Hayward et al. in silica nanostructures templated by poly(styrene-d_8)-*block*-poly(2-vinylpyridine) with a poly(2-vinylpyridine) matrix swollen in HCl(aq).[48]

Encouraged by this somewhat unexpected finding, we sought a melt-processable HEX-forming block copolymer that would

https://doi.org/10.1021/acs.nanolett.1c02097
Nano Lett. 2021, 21, 7587−7594

yield a mechanically tough material upon matrix domain etching. We consequently investigated the fabrication of nanoporous polymers derived from 1,4-polyisoprene-*block*-polylactide (PI-*b*-PLA), in which the PI cylinders are thermally cross-linked with dicumyl peroxide (DCP) during melt processing to enhance their rigidity (Figure 2a). By a literature

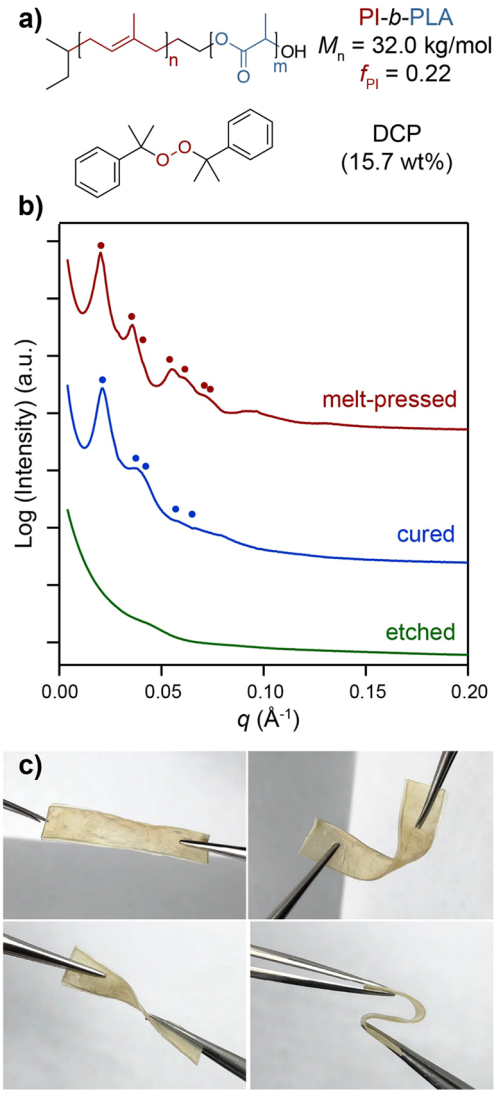

Figure 2. (a) Chemical structure of PI-*b*-PLA and the thermal cross-linker DCP. (b) SAXS patterns of PI-*b*-PLA block polymer loaded with 15.7 wt % DCP before (melt-pressed; red) and after (cured; blue) thermally activated cross-linking of the PI domains. Markers indicate the positions of the expected peaks for hexagonally packed cylinders situated at q^*, $q^*\sqrt{3}$, $q^*\sqrt{4}$, $q^*\sqrt{7}$, $q^*\sqrt{9}$, ...The wet PI-*b*-PLA sample after etching (green) exhibits only a single, broad, and weak correlation peak at q^* = 0.0428 Å^{-1}. (c) Photographs of etched and water-imbibed flexible nanoporous PI which demonstrate that it can be bent, folded, and twisted.

procedure,[49] we synthesized a PI-*b*-PLA diblock with M_n = 32.0 kg/mol ($Đ = M_w/M_n$ = 1.17) and PI volume fraction f_{PI} = 0.22 (see Figures S1c,d and S3 for detailed synthesis and characterization). This polymer was blended with DCP by codissolution in C_6H_6, followed by freeze-drying the mixture to yield a final DCP content of 15.7 wt % as determined via ^{1}H NMR. The resulting mixture was initially compression molded at 60 °C to agglomerate the polymer into a 0.7 mm thick film above the PLA glass transition temperature $T_{g,PLA}$ = 42 °C (which is depressed from 58 °C by DCP blending) without activating the cross-linker. PI microdomain cross-linking was then achieved under hydraulic compression (40 psi) at 155 °C for 1 h. SAXS analyses presented in Figure 2b demonstrate the formation of a HEX morphology in this PI-*b*-PLA/DCP blend prior to cross-linking, evidenced by scattering maxima at $(q/q^*)^2$ = 1, 3, 4, 7, 9, 12, 13, etc. with the microdomain spacing d = 30.7 nm (q^* = 0.0204 Å^{-1}). Cross-linking decreases the d spacing to d = 29.3 nm with some loss of translational order evidenced by higher-order SAXS peak broadening (Figure 2b), due to volume contraction stemming from conversion of van der Waals contacts between the PI segments into covalent cross-links. A comparative SAXS analysis of the neat PI-*b*-PLA diblock (Figure S4) reveals that the incorporation of DCP prior to cross-linking drives a 3% reduction in the observed HEX d-spacing, indicating that DCP compatibilizes the PI and PLA segments by nonselectively partitioning into both domains.[50] Thus, we hereafter assume that the overall f_{PLA} value is not appreciably changed by the inclusion of DCP.

Etching of the cross-linked PI-*b*-PLA film with 2.5 M NaOH in MeOH/H_2O (20/80 v/v) solution at 45 °C for 12 h followed by immersion in DI water to remove the base yields a flexible, water-imbibed nanoporous PI (npPI) monolith that retains its original shape, and it may be bent, twisted, and folded as pictured in Figure 2c. Thus, this wet npPI monolith does not simply fall apart as anticipated by conventional wisdom, since the cylinders apparently remain interconnected. However, monoliths thus prepared become brittle upon drying. Gravimetry reveals that the etching process causes an average mass loss of 81.0 ± 1.0 wt % (five replicates) for the dried npPI, which is somewhat less than the 82.8 wt % loss expected on the basis of the PI-*b*-PLA block copolymer composition. In order to more accurately quantify the mass loss corresponding to etched PLA and to account for contributions from residual DCP, etching was separately performed on cross-linked PI-*b*-PLA samples initially swelled in THF at 55 °C to extract residual DCP and cross-linking byproducts (see the Supporting Information for experimental details). When the THF-extracted, cross-linked PI-*b*-PLA was etched under the same conditions as above, a mass loss of 80.3 ± 0.2 wt % with respect to the extracted cross-linked diblock was determined via triplicate gravimetric measurements. Thus, we deduce that the upper bound on the residual PLA content in the dry porous polymer is 12.6 ± 0.8 wt %, on the basis of the PLA weight fraction of 82.8 wt % in the diblock precursor. Thermogravimetric analysis (TGA) corroborates the presence of ∼12 wt % of PLA in the extracted and dried npPI sample (Figure S5), albeit as an upper-bound value due to uncertainties associated with residual water and DCP decomposition products in the sample. Increasing the etching time to 2−3 days failed to further reduce the PLA content. Since the interfacial width in the PI-PLA HEX morphology is finite, we surmise that some of the DCP initiator reacts with the PLA chains by H-atom abstraction to generate α-enolic radicals[51,52] that cross-link to interfacially mixed PI segments.[53] Thus, PLA is covalently incorporated at or near the surface of the cross-linked PI cylinders, as suggested from FTIR spectra of the etched monolith (see Figure S6).

The cross-linked npPI monoliths imbibed with water were cryofractured and cross-sectionally imaged by SEM (Figure 3a,b) to reveal a porous structure with interconnected polymer fibrils, akin to a previously reported nanoporous PI derived

https://doi.org/10.1021/acs.nanolett.1c02097
Nano Lett. 2021, 21, 7587−7594

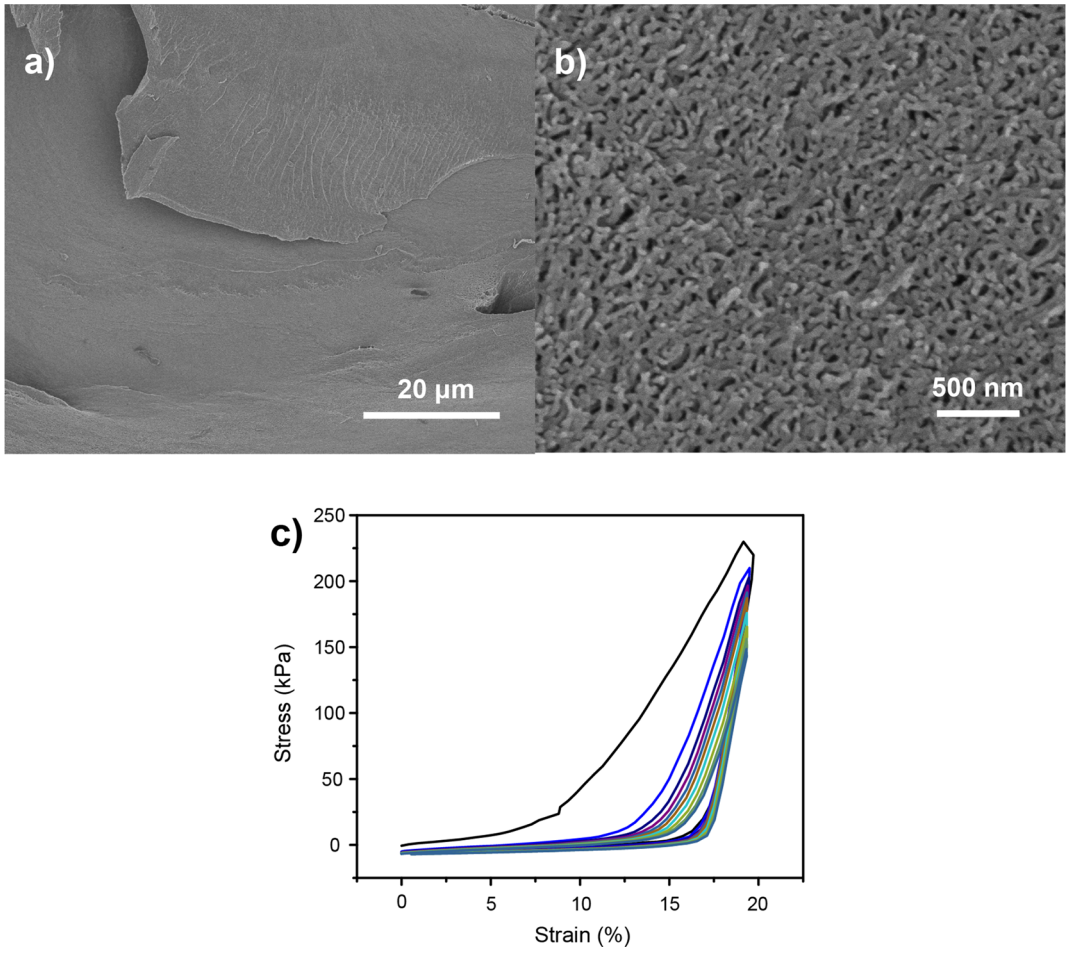

Figure 3. SEM images of the cross-section of a cryofractured npPI sample under (a) low magnification and (b) high magnification, demonstrating the porous structure with interconnected cylindrical fibrils. (c) Cyclic compression of the npPI polymer. Compression moduli were calculated from the two linear regimes of the second compression curve as 95.5 ± 23.9 and 3.58 ± 0.31 MPa, respectively. The maximum normal stress decreases by 26 ± 9% after 10 compression cycles at a maximum strain of 20%. Reported data and standard deviations reflect the results of five independent trials.

from cross-linking and etching a bicontinuous microemulsion.[32] Quantitative image analyses of Figure 3b with ImageJ software indicate the presence of discrete fibers with an average diameter of 16 ± 2 nm, based on 40 measurements of manually selected, isolated fibrils to avoid merged cylinder bundles. This fibril diameter concurs with the expected PI cylinder diameter of 17.4 nm geometrically estimated from the SAXS-derived d = 29.3 nm of the cross-linked PI-*b*-PLA and the total volume occupied by the cross-linked PI and residual PLA in the sample (see Figure S7 for calculation details). In spite of their derivation from an ordered block copolymer morphology, these fibrils are randomly oriented with scant hexatic order and some degree of fibril agglomeration and collapse. This last finding is consistent with the SAXS pattern from the etched, water-filled polymer monolith (Figure 2b), in which the primary scattering peak of the cross-linked PI-PLA sample (q^* = 0.0204 Å^{-1}) transforms into a weak and broad correlation peak (q^* = 0.0428 Å^{-1}) with no higher-order Bragg scattering. This SAXS result, which is similar to that observed on etching PS/PLA RECNs with $f_{PS} \leq 0.35$ by Zeng and Hayward, suggests some degree of rearrangement and collapse of the cross-linked PI domains upon PLA removal.[54] Mass loss quantitation on water removal by drying the porous fibrillar network leads us to estimate its void fraction to be 55 ± 4%. This porosity estimate is lower than the f_{PLA} value of 0.78, also suggesting partial collapse of the cylinders on PLA matrix etching. We note that the obtained porosity is comparable to that reported by Vidil et al. from etching melt-disordered block polymers.[37] The dried samples can be partially rehydrated in DI water to a water content of 40 ± 4 vol %, which implies the modest hydrophilicity of the npPI. This apparent porosity reduction suggests that exhaustive water removal irreversibly alters the nanoporous material structure. Thus, etched npPI samples were subsequently stored in H_2O and characterized in their fully hydrated state unless noted.

The compressive mechanical properties of water-filled npPI samples were characterized by 10 consecutive compression−release cycles with a maximum 20% applied strain at a 0.02 s^{-1} strain rate (Figure 3c). We observe notable hysteresis after the first compression cycle, which likely arises from irreversible plastic deformation and possible collapse of the porous structure. From the slope of the linear regime of the second compression stress−strain curve, we calculate that the compressive modulus of the etched polymer is 95.5 ± 23.9 kPa. The compression profiles obtained in cycles 2−10 exhibit a sharp upturn between 15 and 20% strain, which coincides with that observed in fibrillar network mechanics documented in soft fatty tissue.[55] The fibrillar npPI network mechanics

https://doi.org/10.1021/acs.nanolett.1c02097
Nano Lett. 2021, 21, 7587−7594

continue to evolve such that the peak normal stress decreases by 26 ± 9% after 10 loading cycles, due to some degree of network rupture and possible water loss.

In order to quantify the effective npPI pore size and directly demonstrate pore percolation through a macroscopic film, we examined its performance as a semipermeable membrane for the separation of a mixture of five narrow-dispersity poly(ethylene oxide) (PEO) standards with M_n = 0.4−35 kg/mol at 22 °C. These measurements relied on a U-tube diffusion cell (see Figure S8 and associated description), wherein a 0.35 mm thick npPI membrane was situated between a reservoir containing pure DI water and one containing a mixture of PEO standards with a concentration of 6 mg/mL for each M_n value. Our initial experiment in pure DI water revealed osmotically-driven water transport evident from changes in the water levels on both sides of the membrane. However, only slow and M_n-independent permeation of the PEO (<5 wt %) was observed with little evolution in time. Given the presence of residual PLA in the npPI that could hydrolyze to yield −COOH functionalities lining the fibrillar network surface which bind PEO,[56] we speculated that this slow permeation stemmed from PEO adsorption within the material that clogged the membrane. Consequently, we conducted the same U-tube diffusion experiment after replacing the deionized water with 1.0 M KOH(aq) (pH 14) to promote the deprotonation of any carboxylic acidic functionalities. This condition could additionally promote electrostatic repulsions between the cylindrical fibrils to furnish enhanced porosity.

Figure 4a depicts the time-dependent PEO concentration profiles determined by quantitative SEC analyses of aliquots taken from both arms of the U-tube (see the Supporting Information for details), from which we deduce the percent rejection of PEO by the npPI membrane as shown in Figure 4b. While solvated PEOs with $M_n \leq 1.5$ kg/mol diffuse through the npPI by day 3 of the experiment, ∼98% of the 35 kg/mol PEO was rejected even after 70 days. Thus, the critical pore diameter in the npPI is estimated to be 5.7 nm on the basis of the hydrodynamic radius of 35 kg/mol PEO.[57] This value matches reasonably well with the estimated critical pore size of 4.2 nm estimated from the cylinder diameter including the putative PLA shell, the 55 vol % porosity determined by gravimetry above, and a local hexatic packing of the fibrils (see Figure S9 for a detailed geometrical calculation). The fact that the PEO chains permeate through a macroscopic npPI film confirms the percolating pore structure, suggesting potential nanofiltration applications for these materials.

As a step to better understand the limits within which the mechanical properties of these porous fibrillar networks could be tuned, we attempted to fabricate npPI samples by chemically etching PI-*b*-PLA cross-linked by the above protocol with 8.6, 5.9, and 3.5 wt % of DCP. Samples comprising [DCP] ≤ 5.9 wt % resisted etching even after 2 days, evidenced by only ∼2 wt % mass loss on drying samples exposed to a caustic aqueous solution. SEM analyses of such samples (Figure 5a) revealed the formation of a rough and apparently nonporous structure, which may originate from insufficient cross-linking of the PI to yield high-modulus fibrils. We surmise that the collapsed PI fibrils most likely form a rubbery barrier layer around the macroscopic sample that prevents complete etching. This result is in contrast with the porous structures of the npPI samples obtained using [DCP] = 8.6 wt % (Figure 5b). This line of reasoning is consistent with the notion that preventing porous polymer nanostructure

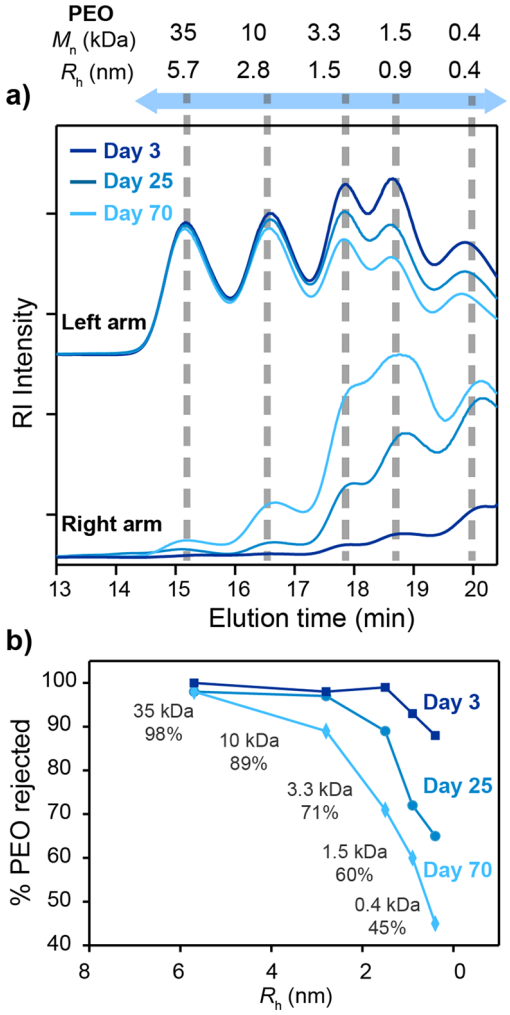

Figure 4. (a) SEC traces showing the time evolution of the polymer concentrations in the PEO stock solution (left arm, top) and the blank solution (right arm, bottom), which are separated by a semipermeable npPI membrane in a U-tube apparatus. Dashed lines indicate the molar mass and hydrodynamic radius of each PEO standard. (b) Percentage of PEO rejected by the npPI membrane as a function of PEO hydrodynamic radius (R_h) after 3, 25, and 70 days of permeation.

collapse requires the polymer modulus to be sufficiently high to counteract the Laplace pressure within the nanopores.[29,58] The cross-linked, higher T_g PLA layer coating the elastomeric PI cylinders in a putative core−shell structure may also aid the preservation of the structural porosity and enhance npPI mechanical stability.

Although one does not intuitively expect etching the matrix domain of a block copolymer HEX morphology to produce a bicontinuous, nanoporous material, our findings demonstrate that the minority-phase cylinders are connected. The expectation that matrix etching would yield only cylindrical fibrils that fall apart is predicated on a pseudo-single-domain sample and neglects the existence of grain boundaries and their detailed structures. In concurrence with the latter expectation, Stamm and co-workers demonstrated that a pseudo-single-domain sample of a diblock copolymer HEX morphology produced by shear processing may be dissolved into isolated nanocylinders.[46] Transmission electron microtomography studies by Jinnai et al.[59] have documented connections

https://doi.org/10.1021/acs.nanolett.1c02097
Nano Lett. 2021, 21, 7587−7594

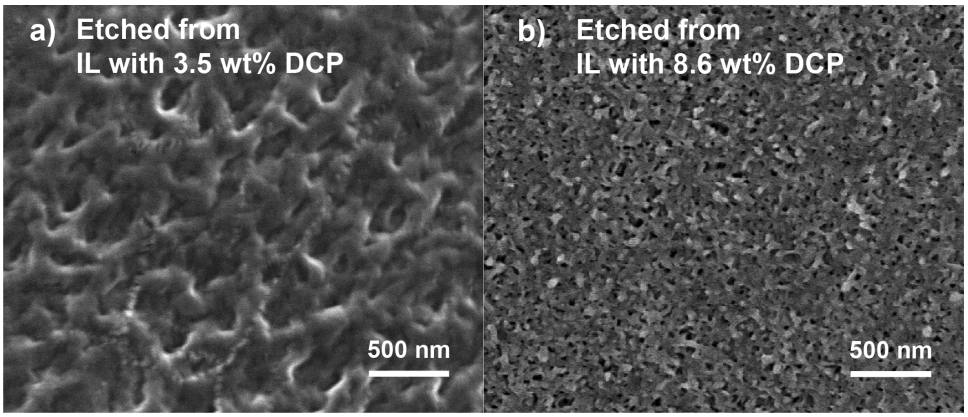

Figure 5. SEM images of (a) an etched PI-*b*-PLA sample cured with 3.5 wt % DCP, showing the surface after immersion in 2.5 M NaOH in MeOH/H_2O (20/80 v/v) at 45 °C for 2 days and (b) a cryofractured npPI sample with 8.6 wt % DCP demonstrating its porous cross section.

between the cylinders in adjacent, randomly oriented grains of a HEX-forming polystyrene-*block*-polyisoprene diblock as a type of topological defect. Even pseudo-single-domain HEX morphologies produced by shear alignment possess Y junctions (branches) as common defects in imperfectly aligned specimens.[26] Thus, cross-linking the interconnected cylinders in randomly oriented HEX grains leads to a percolating yet porous fibrillar network with reasonable mechanical properties. The stability of these npPI monoliths in aqueous media suggests that the residual hydrophilic hydroxyl and carboxylate functionalities on the cylinder surfaces do not appreciably contribute to monolith cohesion. Additionally, hydrophobic associations between the cylinders contribute only negligibly to the monolith stability, as such interactions would be expected to drive more complete pore collapse on dehydration, which is at odds with the above observations. The percolating nature of the cross-linked network is instead evident in the lack of solubility of the npPI in THF, an organic solvent that would disrupt hydrophobic associations and solvate the cross-linked PI cylinders. The above results conceptually resemble recent reports from Osuji and co-workers, in which mechanically stable porous ultrafiltration membranes were prepared by cross-linking shear-aligned, cylindrical surfactant micelles in a continuous aqueous matrix.[60,61] The mechanical stability of their micellar network stems from a water-soluble cross-linker that links the fibrils to resist structural change. Our findings regarding the intrinsic continuity of the cylinders through grain boundaries suggest new design principles for other mechanically stable porous materials derived from this simple and scalable preparation process.

In summary, we have demonstrated the preparation of a flexible, nanoporous material by cross-linking of the minority domain of a microphase separated block copolymer HEX morphology followed by matrix domain etching. Contrary to the expectation that discontinuous cylindrical domains would fall apart upon chemical degradation of the matrix phase, we obtained freestanding, cross-linked polymer monoliths that exhibit mechanical properties consistent with the nanofibrillar network morphology observed by SEM. We demonstrated the percolating nanoporosity of the resulting materials by selective permeation of solvated PEO samples of varying molar masses, which enabled deduction of a critical pore size that conforms to expectations based on SAXS analyses of the block copolymer precursors. These findings highlight how finite-sized grains in the HEX morphology and the structures of their grain boundaries unexpectedly pave the way toward the simple and scalable preparation of nanoporous polymers with potentially tunable surface activities, void sizes, and mechanical properties.

■ ASSOCIATED CONTENT

Supporting Information

The Supporting Information is available free of charge at https://pubs.acs.org/doi/10.1021/acs.nanolett.1c02097.

Polymer synthesis and characterization methods, detailed procedure for U-tube permeation experiments, and detailed calculations of the pore dimensions in npPI (PDF)

■ AUTHOR INFORMATION

Corresponding Authors

Christopher J. Ellison − *Department of Chemical Engineering & Materials Science, University of Minnesota, Minneapolis, Minnesota 55455, United States;* orcid.org/0000-0002-0393-2941; Phone: +1 (612) 626-9834; Email: cellison@umn.edu

Mahesh K. Mahanthappa − *Department of Chemical Engineering & Materials Science, University of Minnesota, Minneapolis, Minnesota 55455, United States;* orcid.org/0000-0002-9871-804X; Phone: +1 (612) 625-4599; Email: maheshkm@umn.edu

Authors

Hongyun Xu − *Department of Chemical Engineering & Materials Science, University of Minnesota, Minneapolis, Minnesota 55455, United States;* orcid.org/0000-0002-2406-9024

Han Xiao − *Department of Chemical Engineering & Materials Science, University of Minnesota, Minneapolis, Minnesota 55455, United States*

Complete contact information is available at: https://pubs.acs.org/10.1021/acs.nanolett.1c02097

Author Contributions

The manuscript was written through contributions of all authors. All authors have given approval to the final version of the manuscript.

Notes

The authors declare no competing financial interest.

https://doi.org/10.1021/acs.nanolett.1c02097
Nano Lett. 2021, 21, 7587−7594

■ ACKNOWLEDGMENTS

This work was funded by National Science Foundation grants DMR-1708874 and DMR-2003668 and start-up funds from the Department of Chemical Engineering & Materials Science and College of Science & Engineering at the University of Minnesota. Synchrotron SAXS patterns were collected at the 12-ID-B beamline of the Advanced Photon Source, a U.S. Department of Energy (DOE) Office of Science User Facility operated by Argonne National Laboratory under contract no. DE-AC02-06CH11357. Portions of this work were carried out at the Characterization Facility at the University of Minnesota, which receives partial support from the NSF through the MRSEC (Award Number DMR-2011401) and the NNCI (Award Number ECCS-2025124) programs. We thank Aaron Lindsay for kindly providing the α-hydroxy-polystyrene (PS-OH) and α-hydroxy-polyisoprene (PI-OH) precusors used in this study.

■ REFERENCES

(1) Park, M.; Harrison, C.; Chaikin, P. M.; Register, R. A.; Adamson, D. H. Block Copolymer Lithography: Periodic Arrays of ~ 10^{11} Holes in 1 Square Centimeter. *Science* **1997**, *276*, 1401−1404.
(2) Bang, J.; Jeong, U.; Ryu, D. Y.; Russell, T. P.; Hawker, C. J. Block Copolymer Nanolithography: Translation of Molecular Level Control to Nanoscale Patterns. *Adv. Mater.* **2009**, *21*, 4769−4792.
(3) Bates, C. M.; Maher, M. J.; Janes, D. W.; Ellison, C. J.; Willson, C. G. Block Copolymer Lithography. *Macromolecules* **2014**, *47*, 2−12.
(4) Carter, K. R.; DiPietro, R. A.; Sanchez, M. I.; Swanson, S. A. Nanoporous Polyimides Derived from Highly Fluorinated Polyimide/Poly(propylene oxide) Copolymers. *Chem. Mater.* **2001**, *13*, 213−221.
(5) Yang, S. Y.; Ryu, I.; Kim, H. Y.; Kim, J. K.; Jang, S. K.; Russell, T. P. Nanoporous Membranes with Ultrahigh Selectivity and Flux for the Filtration of Viruses. *Adv. Mater.* **2006**, *18*, 709−712.
(6) Phillip, W. A.; O'neill, B.; Rodwogin, M.; Hillmyer, M. A.; Cussler, E. L. Self-Assembled Block Copolymer Thin Films as Water Filtration Membranes. *ACS Appl. Mater. Interfaces* **2010**, *2*, 847−853.
(7) Rolison, D. R. Catalytic Nanoarchitectures–the Importance of Nothing and the Unimportance of Periodicity. *Science* **2003**, *299*, 1698.
(8) Liu, F.; Kong, W.; Qi, C.; Zhu, L.; Xiao, F.-S. Design and Synthesis of Mesoporous Polymer-Based Solid Acid Catalysts with Excellent Hydrophobicity and Extraordinary Catalytic Activity. *ACS Catal.* **2012**, *2*, 565−572.
(9) Xu, Y.; Gu, W.; Gin, D. L. Heterogeneous Catalysis Using a Nanostructured Solid Acid Resin Based on Lyotropic Liquid Crystals. *J. Am. Chem. Soc.* **2004**, *126*, 1616−1617.
(10) Gupta, P.; Paul, S. Solid Acids: Green Alternatives for Acid Catalysis. *Catal. Today* **2014**, *236*, 153−170.
(11) Jones, B. H.; Lodge, T. P. Nanocasting Nanoporous Inorganic and Organic Materials from Polymeric Bicontinuous Microemulsion Templates. *Polym. J.* **2012**, *44*, 131−146.
(12) Choi, J. W.; Li, Z.; Black, C. T.; Sweat, D. P.; Wang, X.; Gopalan, P. Patterning at the 10 Nanometer Length Scale Using a Strongly Segregating Block Copolymer Thin Film and Vapor Phase Infiltration of Inorganic Precursors. *Nanoscale* **2016**, *8*, 11595−11601.
(13) Vakifahmetoglu, C.; Zeydanli, D.; Colombo, P. Porous Polymer Derived Ceramics. *Mater. Sci. Eng., R* **2016**, *106*, 1−30.
(14) Liang; George, S. M.; Weimer, A. W.; Li, N.-H.; Blackson, J. H.; Harris, J. D.; Li, P. Synthesis of a Novel Porous Polymer/Ceramic Composite Material by Low-Temperature Atomic Layer Deposition. *Chem. Mater.* **2007**, *19*, 5388−5394.
(15) Yang, S. Y.; Yang, J. A.; Kim, E. S.; Jeon, G.; Oh, E. J.; Choi, K. Y.; Hahn, S. K.; Kim, J. K. Single-File Diffusion of Protein Drugs through Cylindrical Nanochannels. *ACS Nano* **2010**, *4*, 3817−3822.
(16) Rzayev, J.; Hillmyer, M. A. Nanochannel Array Plastics with Tailored Surface Chemistry. *J. Am. Chem. Soc.* **2005**, *127*, 13373−13379.
(17) Bailey, T. S.; Rzayev, J.; Hillmyer, M. A. Routes to Alkene and Epoxide Functionalized Nanoporous Materials from Poly(styrene-*b*-isoprene-*b*-lactide) Triblock Copolymers. *Macromolecules* **2006**, *39*, 8772−8781.
(18) Mao, H.; Arrechea, P. L.; Bailey, T. S.; Johnson, B. J. S.; Hillmyer, M. A. Control of Pore Hydrophilicity in Ordered Nanoporous Polystyrene Using an AB/AC Block Copolymer Blending Strategy. *Faraday Discuss.* **2005**, *128*, 149−162.
(19) Hawker, C. J.; Wooley, K. L. The Convergence of Synthetic Organic and Polymer Chemistries. *Science* **2005**, *309*, 1200−1205.
(20) Hillmyer, M. A. Nanoporous Materials from Block Copolymer Precursors. *Adv. Polym. Sci.* **2005**, *190*, 137−181.
(21) Abetz, V.; Simon, P. F. W. Phase Behaviour and Morphologies of Block Copolymers. *Adv. Polym. Sci.* **2005**, *189*, 125−212.
(22) Bates, C. M.; Bates, F. S. Block Polymers—Pure Potential. *Macromolecules* **2017**, *50*, 3−22.
(23) Olson, D. A.; Chen, L.; Hillmyer, M. A. Templating Nanoporous Polymers with Ordered Block Copolymers. *Chem. Mater.* **2008**, *20*, 869−890.
(24) Jackson, E. A.; Hillmyer, M. A. Nanoporous Membranes Derived from Block Copolymers: From Drug Delivery to Water Filtration. *ACS Nano* **2010**, *4*, 3548−3553.
(25) Lee, J. S.; Hirao, A.; Nakahama, S. Polymerization of Monomers Containing Functional Silyl Groups. 5. Synthesis of New Porous Membranes with Functional Groups. *Macromolecules* **1988**, *21*, 274−276.
(26) Zalusky, A. S.; Olayo-Valles, R.; Wolf, J. H.; Hillmyer, M. A. Ordered Nanoporous Polymers from Polystyrene-Polylactide Block Copolymers. *J. Am. Chem. Soc.* **2002**, *124*, 12761−12773.
(27) Mao, H.; Hillmyer, M. A. Nanoporous Polystyrene by Chemical Etching of Poly(ethylene oxide) from Ordered Block Copolymers. *Macromolecules* **2005**, *38*, 4038−4039.
(28) Ndoni, S.; Vigild, M. E.; Berg, R. H. Nanoporous Materials with Spherical and Gyroid Cavities Created by Quantitative Etching of Polydimethylsiloxane in Polystyrene−Polydimethylsiloxane Block Copolymers. *J. Am. Chem. Soc.* **2003**, *125*, 13366−13367.
(29) Cavicchi, K. A.; Zalusky, A. S.; Hillmyer, M. A.; Lodge, T. P. An Ordered Nanoporous Monolith from an Elastomeric Crosslinked Block Copolymer Precursor. *Macromol. Rapid Commun.* **2004**, *25*, 704−709.
(30) Hashimoto, T.; Tsutsumi, K.; Funaki, Y. Nanoprocessing Based on Bicontinuous Microdomains of Block Copolymers: Nanochannels Coated with Metals. *Langmuir* **1997**, *13*, 6869−6872.
(31) Mao, H.; Hillmyer, M. A. Macroscopic Samples of Polystyrene with Ordered Three-Dimensional Nanochannels. *Soft Matter* **2006**, *2*, 57−59.
(32) Zhou, N.; Bates, F. S.; Lodge, T. P. Mesoporous Membrane Templated by a Polymeric Bicontinuous Microemulsion. *Nano Lett.* **2006**, *6*, 2354−2357.
(33) Kanamori, K.; Nakanishi, K.; Hanada, T. Rigid Macroporous Poly(divinylbenzene) Monoliths with a Well-defined Bicontinuous Morphology Prepared by Living Radical Polymerization. *Adv. Mater.* **2006**, *18*, 2407−2411.
(34) Seo, M.; Hillmyer, M. A. Reticulated Nanoporous Polymers by Controlled Polymerization-Induced Microphase Separation. *Science* **2012**, *336*, 1422−1425.
(35) Utroša, P.; Žagar, E.; Kovačič, S.; Pahovnik, D. Porous Polystyrene Monoliths Prepared from *in situ* Simultaneous Interpenetrating Polymer Networks: Modulation of Morphology by Polymerization Kinetics. *Macromolecules* **2019**, *52*, 819−826.
(36) Schulze, M. W.; Hillmyer, M. A. Tuning Mesoporosity in Cross-Linked Nanostructured Thermosets via Polymerization-Induced Microphase Separation. *Macromolecules* **2017**, *50*, 997−1007.
(37) Vidil, T.; Hampu, N.; Hillmyer, M. A. Nanoporous Thermosets with Percolating Pores from Block Polymers Chemically Fixed above the Order-Disorder Transition. *ACS Cent. Sci.* **2017**, *3*, 1114−1120.
(38) Hampu, N.; Bates, M. W.; Vidil, T.; Hillmyer, M. A. Bicontinuous Porous Nanomaterials from Block Polymers Radically

https://doi.org/10.1021/acs.nanolett.1c02097
Nano Lett. 2021, 21, 7587−7594

Cured in the Disordered State for Size-Selective Membrane Applications. *ACS Appl. Nano Mater.* **2019**, *2*, 4567−4577.
(39) Hampu, N.; Hillmyer, M. A. Molecular Engineering of Nanostructures in Disordered Block Polymers. *ACS Macro Lett.* **2020**, *9*, 382−388.
(40) Zeng, D.; Ribbe, A.; Hayward, R. C. Anisotropic and Interconnected Nanoporous Materials from Randomly End-Linked Copolymer Networks. *Macromolecules* **2017**, *50*, 4668−4676.
(41) Matsen, M. W. Effect of Architecture on the Phase Behavior of AB-Type Block Copolymer Melts. *Macromolecules* **2012**, *45*, 2161−2165.
(42) Yan, X.; Liu, G.; Liu, F.; Tang, B. Z.; Peng, H.; Pakhomov, A. B.; Wong, C. Y. Superparamagnetic Triblock Copolymer/Fe_2O_3 Hybrid Nanofibers. *Angew. Chem., Int. Ed.* **2001**, *40*, 3593−3596.
(43) Liu, G.; Yan, X.; Duncan, S. Polystyrene-*block*-Polyisoprene Nanofiber Fractions. 1. Preparation and Static Light-Scattering Study. *Macromolecules* **2002**, *35*, 9788−9793.
(44) Won, Y.-Y.; Davis, H. T.; Bates, F. S. Giant Wormlike Rubber Micelles. *Science* **1999**, *283*, 960−963.
(45) Liu, G. Block Copolymer Nanotubes Derived from Self-Assembly. *Adv. Polym. Sci.* **2008**, *220*, 29−64.
(46) Fahmi, A. W.; Braun, H.-G.; Stamm, M. Fabrication of Metallized Nanowires from Self-Assembled Diblock Copolymer Templates. *Adv. Mater.* **2003**, *15*, 1201−1204.
(47) Bendejacq, D.; Joanicot, M.; Ponsinet, V. Pearling Instabilities in Water-Dispersed Copolymer Cylinders with Charged Brushes. *Eur. Phys. J. E: Soft Matter Biol. Phys.* **2005**, *17*, 83−92.
(48) Hayward, R. C.; Chmelka, B. F.; Kramer, E. J. Template Cross-Linking Effects on Morphologies of Swellable Block Copolymer and Mesostructured Silica Thin Films. *Macromolecules* **2005**, *38*, 7768−7783.
(49) Schmidt, S. C.; Hillmyer, M. A. Synthesis and Characterization of Model Polyisoprene-Polylactide Diblock Copolymers. *Macromolecules* **1999**, *32*, 4794−4801.
(50) Hanley, K. J.; Lodge, T. P.; Huang, C.-I. Phase Behavior of a Block Copolymer in Solvents of Varying Selectivity. *Macromolecules* **2000**, *33*, 5918−5931.
(51) Rytlewski, P.; Zenkiewicz, M.; Malinowski, R. Influence of Dicumyl Peroxide Content on Thermal and Mechanical Properties of Polylactide. *Int. Polym. Process.* **2011**, *26*, 580−586.
(52) Huang, Y.; Zhang, C.; Pan, Y.; Wang, W.; Jiang, L.; Dan, Y. Study on the Effect of Dicumyl Peroxide on Structure and Properties of Poly(lactic acid)/Natural Rubber Blend. *J. Polym. Environ.* **2013**, *21*, 375−387.
(53) Sunday, D. F.; Maher, M. J.; Hannon, A. F.; Liman, C. D.; Tein, S.; Blachut, G.; Asano, Y.; Ellison, C. J.; Willson, C. G.; Kline, R. J. Characterizing the Interface Scaling of High χ Block Copolymers near the Order−Disorder Transition. *Macromolecules* **2018**, *51*, 173−180.
(54) Zeng, D.; Hayward, R. C. Effects of Randomly End-Linked Copolymer Network Parameters on the Formation of Disordered Cocontinuous Phases. *Macromolecules* **2019**, *52*, 2642−2650.
(55) van Oosten, A. S. G.; Chen, X.; Chin, L.; Cruz, K.; Patteson, A. E.; Pogoda, K.; Shenoy, V. B.; Janmey, P. A. Emergence of Tissue-Like Mechanics from Fibrous Networks Confined by Close-Packed Cells. *Nature* **2019**, *573*, 96−101.
(56) Seo, J.; Lutkenhaus, J. L.; Kim, J.; Hammond, P. T.; Char, K. Development of Surface Morphology in Multilayered Films Prepared by Layer-by-Layer Deposition Using Poly(acrylic acid) and Hydrophobically Modified Poly(ethylene oxide). *Macromolecules* **2007**, *40*, 4028−4036.
(57) Devanand, K.; Selser, J. C. Asymptotic Behavior and Long-Range Interactions in Aqueous Solutions of Poly(ethylene oxide). *Macromolecules* **1991**, *24*, 5943−5947.
(58) Muralidharan, V.; Hui, C.-Y. Stability of Nanoporous Materials. *Macromol. Rapid Commun.* **2004**, *25*, 1487−1490.
(59) Jinnai, H.; Yasuda, K.; Nishi, T. Three-Dimensional Observations of Grain Boundary Morphologies in a Cylinder-Forming Block Copolymer. *Macromol. Symp.* **2006**, *245*−*246*, 170−174.
(60) Feng, X.; Imran, Q.; Zhang, Y.; Sixdenier, L.; Lu, X.; Kaufman, G.; Gabinet, U.; Kawabata, K.; Elimelech, M.; Osuji, C. O. Precise Nanofiltration in a Fouling-Resistant Self-Assembled Membrane with Water-Continuous Transport Pathways. *Sci. Adv.* **2019**, *5*, eaav9308.
(61) Zhang, Y.; Dong, R.; Gabinet, U. R.; Poling-Skutvik, R.; Kim, N. K.; Lee, C.; Imran, O. Q.; Feng, X.; Osuji, C. O. Rapid Fabrication by Lyotropic Self-Assembly of Thin Nanofiltration Membranes with Uniform 1 Nanometer Pores. *ACS Nano* **2021**, *15*, 8192−8203.

https://doi.org/10.1021/acs.nanolett.1c02097
Nano Lett. 2021, 21, 7587−7594